



1 **Large-Scale Vertical Velocity, Diabatic Heating and Drying**
2 **Profiles Associated with Seasonal and Diurnal Variations of**
3 **Convective Systems Observed in the GoAmazon2014/5**
4 **Experiment**

5 Shuaiqi Tang¹, Shaocheng Xie¹, Yunyan Zhang¹, Minghua Zhang², Courtney Schumacher³,
6 Hannah Upton³, Michael P. Jensen⁴, Karen L. Johnson⁴, Meng Wang⁴, Maike Ahlgrimm⁵, Zhe
7 Feng⁶, Patrick Minnis⁷ and Mandana Thieman⁸

8 ¹Lawrence Livermore National Laboratory, Livermore, CA, 94550, USA

9 ²School of Marine and Atmospheric Sciences, Stony Brook University, Stony Brook, NY, 11794, USA

10 ³Department of Atmospheric Sciences, Texas A&M University, College Station, TX, 77843, USA

11 ⁴Brookhaven National Laboratory, Upton, NY, 11973, USA

12 ⁵European Centre for Medium-Range Weather Forecasts, Shinfield Park, Reading RG2 9AX, United Kingdom

13 ⁶Pacific Northwest National Laboratory, Richland, Washington, 99354, USA

14 ⁷NASA Langley Research Center, Hampton, VA, 23681, USA

15 ⁸Science Systems and Applications, Inc, Hampton, VA 23666, USA

16 *Correspondence to:* Shuaiqi Tang (tang32@llnl.gov)

17 **Abstract.** This study describes the characteristics of large-scale vertical velocity, apparent
18 heating source (Q_1) and apparent moisture sink (Q_2) profiles associated with seasonal and diurnal
19 variations of convective systems observed during the two intensive operational periods (IOPs) of
20 the Green Ocean Amazon (GoAmazon2014/5) experiment, which was conducted near Manaus,
21 Brazil in 2014 and 2015. The derived large-scale fields have large diurnal variations according
22 to convective activity in the GoAmazon region and the morning profiles show distinct
23 differences between the dry and wet seasons. In the wet season, propagating convective systems
24 originating far from the GoAmazon region are often seen in the early morning, while in the dry
25 season, they are rarely observed. Afternoon convective systems due to solar heating are
26 frequently seen in both seasons. Accordingly, in the morning, there is strong upward motion and
27 associated heating and drying throughout the entire troposphere in the wet season, which is
28 limited to lower levels in the dry season. In the afternoon, both seasons exhibit weak heating and
29 strong moistening in the boundary layer related to the vertical convergence of eddy fluxes. A set



30 of case studies of three typical types of convective systems occurring in Amazonia - i.e., locally-
31 occurring systems, coastal-occurring systems and basin-occurring systems - is also conducted to
32 investigate the variability of the large-scale environment with different types of convective
33 systems.



34 **1. Introduction**

35 Amazonia is one of the major tropical convective regions in the global climate system. It
36 provides moisture to the global hydrological cycle and energy to drive the global atmospheric
37 circulation. Understanding convective systems over the Amazon region through observations is
38 important for understanding and simulating global circulation and climate. However, most of
39 Amazonia is covered by tropical forest with only a few observational sites. In order to collect
40 the observations needed to improve our understanding of convective systems over Amazonia,
41 several major field campaigns have been conducted in this area such as the Amazon Boundary
42 Layer Experiments (Harriss et al., 1988; Harriss et al., 1990), the Large-Scale Biosphere-
43 Atmosphere Experiment in Amazonia (LBA) (Silva Dias et al., 2002b), and the CHUVA project
44 (Machado et al., 2014).

45 Recently, an internationally collaborative experiment, the Observations and Modeling of
46 the Green Ocean Amazon (GoAmazon2014/5) (Martin et al., 2016), was conducted in the region
47 around Manaus, Brazil from January 2014 to December 2015 with a focus on the aerosol and
48 cloud life cycles and aerosol-cloud-precipitation interactions over tropical rainforests. Two 40-
49 day Intensive Operational Periods (IOPs) were conducted to investigate the seasonal variations
50 of clouds and aerosols, as well as their interactions. IOP1 took place from 15 February to 26
51 March 2014 during the wet season, and IOP2 took place from 1 September to 10 October 2014
52 during the dry season. The goal of this study is to document and understand the seasonal
53 variability and diurnal cycle of large-scale vertical velocity, heat and moisture budgets associated
54 with the convective systems observed during the two IOPs in the GoAmazon2014/5 experiment.



55 The Amazon region has a significant seasonal variation in precipitation amount. Rainfall
56 is approximately 300 mm per month during the wet season while it is close to 100 mm per month
57 during the dry season (Tanaka et al., 2014). Many studies have examined the seasonal variation
58 of clouds and precipitation in Amazonia (e.g. Fu et al., 2001; Schumacher and Houze, 2003;
59 Machado et al., 2004; Li et al., 2006; Marengo et al., 2012). Compared to the large variation in
60 clouds and rainfall, the seasonal variation in CAPE is small (Machado et al., 2004; Martin et al.,
61 2016), which implies that small perturbations in the large-scale circulation can drive dramatic
62 changes in hydrological fields in this region. Few studies, however, have studied the seasonal
63 variation of the diabatic heating and drying structures associated with the convective systems in
64 the Amazon region.

65 The diurnal cycle of the atmosphere is an important feature that is poorly simulated in
66 climate models. Many efforts have been made to observe and to understand the diurnal cycle
67 over the Amazon basin using surface observations (e.g. Harriss et al., 1990; Cutrim et al., 2000;
68 Machado et al., 2004; Tanaka et al., 2014) or satellite data (e.g. Minnis and Harrison, 1984;
69 Greco et al., 1990; Janowiak et al., 2005; Burleyson et al., 2016). The diurnal cycle over the
70 Amazon basin is complex because it is affected by three types of convective systems: locally-
71 occurring systems (LOS) generated locally in the form of small convective cells (area less than
72 1000 km²) with short life time (on the order of 1 hour), coastal-occurring systems (COS)
73 initialized at the northeast coast of Brazil by the sea-breeze and propagating inland as squall lines,
74 and basin-occurring systems (BOS) initialized in the Amazon basin in the form of mesoscale
75 convective systems (MCS) with areas larger than 1000 km² (Greco et al., 1990). These systems
76 reach Manaus, near the center of the Amazon basin, at different times of the day, causing a broad
77 peak of precipitation from morning to early afternoon (e.g. Machado et al., 2004; Tanaka et al.,



78 2014; Burleyson et al., 2016). Schumacher et al. (2007) examined the diurnal cycle of the large-
79 scale Q_1 budget in the southwest Amazon during LBA, but used only two profiles per day, which
80 do not capture the rapidly changing environment. In addition, the diurnal cycle over the highly
81 deforested southwest Amazon is not necessarily representative of the more pristine central
82 Amazonian rainforest.

83 In this study we use data collected from the comprehensive GoAmazon2014/5 field
84 campaign to examine the seasonal and diurnal variations of the large-scale vertical velocity and
85 heat and moisture budgets associated with the convective systems that occur in central Amazonia.
86 Section 2 provides details of the data and method used to derive the large-scale profiles for the
87 GoAmazon2014/5 experiment. Section 3 describes the synoptic conditions for the two IOPs.
88 Sections 4 and 5 show the seasonal variation and diurnal cycle of the large-scale fields,
89 respectively. Section 6 further investigates three selected cases representing different types of
90 convective systems in the wet season. The summary and discussion are given in Section 7.

91

92 2. Data and Method

93 Due to the lack of an appropriate sounding array to capture the divergence and advection
94 fields in the analysis domain, the large-scale vertical velocity and budgets analyzed in this study
95 were derived by using, as a first guess, the European Centre for Medium-Range Weather
96 Forecasts (ECMWF) analysis data that are subsequently constrained with surface and top of
97 atmosphere (TOA) observations. The upper-level fields from ECMWF analysis data are
98 adjusted to conserve the vertical integration of mass, moisture and dry static energy through a
99 constrained variational analysis technique described in Zhang and Lin (1997) and Zhang et al.



100 (2001). As indicated in Xie et al. (2004), the use of the surface and TOA observations as
101 constraints improves the quality of the large-scale vertical velocity and budgets in operational
102 analysis data and makes the data suitable for budget analysis and cloud modeling studies. An
103 important by-product of this study is the derived large-scale forcing data supporting modeling
104 studies, which are available to the community at the Atmospheric Radiation Measurement (ARM)
105 program Archive (http://iop.archive.arm.gov/arm-iop/0eval-data/xie/scm-forcing/iop_at_mao/).

106 Figure 1 shows the location of the GoAmazon2014/5 experiment and the analysis domain
107 (the red octagon, referred to as the GoAmazon domain) used in this study. The observational
108 research sites and major cities near the region are also shown on the map. The required surface
109 and TOA fluxes as the constraints for the variational analysis are constructed as follows. The
110 precipitation used in this study is derived from the System for the Protection of Amazonia
111 (SIPAM) S-band (10 cm wavelength) radar operated at Ponta Pelada airport, the center of the
112 GoAmazon domain. The SIPAM radar reflectivity constant altitude plan position indicator
113 (CAPPI) at 2.5 km above ground was used to generate the rain rate products using a single Z-R
114 relation of $Z = 174.8R^{1.56}$ derived from Joss-Waldvogel disdrometer data obtained by the
115 CHUVA campaign near Manacapuru during the wet season of early 2014. Other surface
116 constraint variables, such as surface radiative fluxes and latent and sensible heat fluxes, are
117 obtained from the broadband radiometer (ARM Climate Research Facility, 1994) and eddy
118 correlation flux measurement system (ARM Climate Research Facility, 2003) at the ARM
119 Mobile Facility site near Manacapuru (3.213°S, 60.598°W; “ARM site” in Figure 1).
120 Observations of latent and sensible heat fluxes at two other Brazilian research sites - K34
121 (“FLUXNET-BR Ma2” in Figure 1) and the Amazon Tall Tower Observatory (“ATTO Tower”
122 in Figure 1) - are also used. Because of the limited number of surface sites, it is challenging to



123 obtain domain mean fluxes that can well represent the analysis domain. In this study, we use the
124 Cressman's objective analysis method (Cressman, 1959) to incorporate these limited
125 observations into the analysis with the ECMWF analysis as the first guess. The TOA
126 measurements of broadband radiative fluxes are estimated from the Thirteenth Geostationary
127 Operational Environmental Satellite (GOES-13) 4-km visible (0.65 μm) and infrared window
128 (10.8 μm) radiances using the narrowband-to-broadband (NB-BB) conversion method of Minnis
129 and Smith (1998) that was updated similar to Khaiyer et al. (2010), with some modifications to
130 more closely match those measured by the Clouds and Earth's Radiant Energy System (CERES)
131 on the Aqua and Terra satellite. All data are interpolated into 3 h and 25 hPa (if applicable)
132 temporal and vertical resolutions, respectively.

133

134 **3. Background of Synoptic Conditions**

135 The IOP-averaged sea-level pressure and 10-meter horizontal winds from ERA-Interim
136 reanalysis (Dee et al., 2011) are plotted in Figure 2. During IOP1, the Atlantic Intertropical
137 Convergence Zone (ITCZ) was located near the Equator; while during IOP2, it was located near
138 10°N. A fourteen-day trajectory study shows that the air masses over Manaus typically come
139 from the Northern Hemisphere during IOP1 and from the Southern Hemisphere during IOP2
140 (Martin et al., 2016). The top three rows of Figure 3 show the domain-averaged zonal (u) wind,
141 meridional (v) wind, and relative humidity relative to liquid water, from the adjusted ECMWF
142 analysis. Consistent with those derived from radiosonde data in Martin et al. (2016), IOP1 was
143 dominated by northeasterly winds in the lower troposphere, with moist air throughout the



144 troposphere; IOP2 was dominated by easterly winds in the lower troposphere, with a dry free
145 troposphere.

146 The cloud frequency and domain-mean precipitation observed during IOP1 and IOP2 are
147 shown in the remaining two rows of Figure 3. The cloud frequency was derived from the Active
148 Remote Sensing of Clouds (ARSCL) (Kollias et al., 2007) product, which uses a combination of
149 the 95GHz W-band ARM cloud radar (WACR), micropulse lidar (MPL), and ceilometer located
150 at the ARM site to determine a best-estimate cloud mask with 5-second temporal and 30-meter
151 vertical resolution. The ARSCL product leverages each instrument's strengths: the WACR
152 penetrates non-precipitating thick clouds, the MPL is sensitive to thin clouds, and the ceilometer
153 reliably detects cloud base. The ARSCL-derived cloud mask data were then used to produce 3-
154 hourly cloud frequencies following the method described in Xie et al. (2010b). The wet season
155 has more cloud and precipitation events than the dry season. However, the convective systems
156 in the dry season are typically more intense than those occurring in the wet season (Giangrande
157 et al., 2016, accepted). Compared to 15-year climatology, the precipitation around Manaus
158 during 2014 has a positive anomaly in IOP1 and negative anomaly in IOP2 (Burleyson et al.,
159 2016; Martin et al., 2016). Nevertheless, the annual cycle in 2014 is still broadly representative
160 of the climatology (Burleyson et al., 2016).

161

162 **4. Seasonal Variation**

163 In this section, we focus on the contrast between the dry and wet season large-scale
164 vertical velocity and energy and moisture budgets. The upper row of Figure 4 shows the
165 temporal evolution of large-scale vertical velocity in IOP1 (wet season, left) and IOP2 (dry



166 season, right), and the IOP-mean profiles are shown as the black solid lines in the bottom row.
167 We also define rainy (black dotted lines) and non-rain periods (gray lines) using a threshold of
168 0.2 mm hr^{-1} . A value of 0.2 mm hr^{-1} rather than 0 mm hr^{-1} is used because in some cases ground
169 clutter in the SIPAM radar data may be misinterpreted as light precipitation. Changing the
170 threshold affects the magnitude of the vertical profiles but does not change the seasonal contrast
171 and the results of this study. Using this threshold, the percentage of the rainy period to the entire
172 IOP is 36.9% for IOP1, but is 17.8% for IOP2, indicating that the rain frequency is an important
173 factor impacting the seasonal mean contrast. The red and blue lines represent the mean profiles
174 of morning (at 5 local time (LT)) precipitation systems and afternoon (at 14 LT) precipitation
175 systems, respectively, which will be discussed in Section 5.

176 The non-rain vertical velocity profiles are relatively weak, with downward motion
177 dominating in the upper troposphere during both dry and wet seasons. The rainy vertical
178 velocity profiles show strong upward motion throughout the troposphere during both IOPs, but
179 the level of maximum upward motion is different. The upward motion during the rainy period of
180 IOP1 has a broad peak structure from ~ 700 to 300 hPa with the maximum at $\sim 350 \text{ hPa}$. The
181 350-hPa upward motion peak is consistent with that shown in the Tropical Ocean and Global
182 Atmosphere Coupled Ocean-Atmosphere Response Experiment (TOGA COARE) (Lin and
183 Johnson, 1996), but lower than the peak of $\sim 265 \text{ hPa}$ observed in the Tropical Warm Pool-
184 International Cloud Experiment (TWP-ICE) (Xie et al., 2010a). The upward motion during the
185 IOP2 rainy period also has a broad peak but the maximum is at a much lower level ($\sim 550 \text{ hPa}$)
186 than in IOP1. Because the frequency of the rainy period is higher in IOP1 than in IOP2, the IOP-
187 mean upward motion is stronger during IOP1 but weaker and limited to the lower troposphere
188 during IOP2. As discussed in the next section, the difference in morning precipitation systems



189 largely contributes to the seasonal contrast in the vertical velocity profiles between the wet and
 190 dry seasons.

191 Figures 5 and 6 show the temporal evolution and IOP-mean of apparent heating Q_1 and
 192 apparent drying Q_2 profiles, respectively. Q_1 and Q_2 were first introduced by Yanai et al. (1973)
 193 to estimate the diabatic processes:

$$\begin{aligned}
 194 \quad Q_1 &= \frac{\partial \bar{s}}{\partial t} + \bar{V} \cdot \nabla \bar{s} + \bar{\omega} \frac{\partial \bar{s}}{\partial p}, \\
 &= Q_{rad} + L_v (c - e) - \overline{\frac{\partial \omega' s'}{\partial p}}, \quad (1)
 \end{aligned}$$

$$\begin{aligned}
 195 \quad Q_2 &= -L_v \left(\frac{\partial \bar{q}}{\partial t} + \bar{V} \cdot \nabla \bar{q} + \bar{\omega} \frac{\partial \bar{q}}{\partial p} \right), \\
 &= L_v (c - e) + L_v \overline{\frac{\partial \omega' q'}{\partial p}}, \quad (2)
 \end{aligned}$$

196 where $s = C_p T + gz$ is the dry static energy; q is water vapor mixing ratio; \bar{V} is horizontal wind
 197 vector; ω is vertical velocity in pressure coordinate; Q_{rad} is radiative heating; $L_v (c - e)$ is the
 198 latent heat from water condensation and evaporation (in general it also includes the latent heat
 199 and water vapor change from ice phase change); the overbar refers to a horizontal average and
 200 the prime refers to a deviation from the average. Q_1 and Q_2 are calculated from the large-scale
 201 dynamics (the first lines of the equations) and represent the unresolved physical heat sources and
 202 moisture sinks (the second lines). The vertical distributions of heating and drying profiles are
 203 important to the large-scale circulation as discussed in many other studies (e.g. Hartmann et al.,
 204 1984; Lau and Peng, 1987; Puri, 1987; Hack and Schubert, 1990).



205 Similar to the profiles of vertical velocity, non-rain Q_1 and Q_2 profile magnitudes in both
206 IOPs are weak with small amounts of heating and moistening below 600 hPa indicative of non-
207 precipitating or very weakly precipitating shallow cumulus and congestus clouds (Schumacher et
208 al., 2008). Rainy period Q_1 and Q_2 profiles show strong heating and drying throughout the
209 troposphere during both IOPs associated with deep convection, and both of them have double
210 peak structures that vary between dry and wet seasons. Q_1 during IOP1 has a broad primary
211 peak between 600 and 400 hPa, while the primary Q_1 peak during IOP2 maximizes more sharply
212 at 550 hPa. The secondary peaks of Q_1 are at \sim 750 hPa in both IOPs. The peaks of Q_2 in IOP1
213 (at 500 and 750 hPa) are higher than those in IOP2 (at 650 and 800 hPa). The double peak
214 features of Q_1 and Q_2 are likely due to different physical processes. For Q_1 , the local minimum
215 usually occurs near the melting level (\sim 600 hPa), indicating latent cooling due to ice melting.
216 Because the melting level is nearly constant in the tropics, the local minimums of Q_1 are more or
217 less at the same level as seen in other tropical field campaigns (e.g. Schumacher et al., 2008; Xie
218 et al., 2010a). For Q_2 , the double-peak structure is the combined effect of convective (lower
219 peak) and stratiform (higher peak) rain production (Lin and Johnson, 1996). The peak levels for
220 stratiform and convective clouds may vary in different locations and times such as in the two
221 IOPs in this study.

222

223 **5. Diurnal Cycle**

224 The diurnal cycles of domain mean radar-derived precipitation and surface CAPE and
225 convective inhibition (CIN) for both IOPs are plotted in Figure 7. Precipitation in IOP1 extends
226 from early morning to afternoon, consistent with Tanaka et al. (2014). In IOP2, most of the



227 precipitation occurs in the afternoon. The magnitude of afternoon precipitation in IOP2 is just
228 slightly smaller than that in IOP1, but the magnitude of morning precipitation in IOP2 is
229 significantly lower than that in IOP1, indicating that the differences between dry and wet seasons
230 are mainly due to the morning precipitation events. The surface CAPE has similar magnitudes in
231 the daytime during IOP1 and IOP2, but in the early morning it rises later and slower during IOP1
232 than during IOP2, probably because early morning precipitation during IOP1 has released
233 atmospheric instability. The surface CIN is typically small, especially during IOP1, which is due
234 to the high surface relative humidity over the Amazon rainforest.

235 The diurnal cycles of cloud frequency, large-scale vertical velocity, Q_1 , Q_2 and $Q_1 - Q_2$
236 for IOP1 (left) and IOP2 (right) are shown in Figure 8. Derived from Eq. (1) and (2),

$$237 \quad Q_1 - Q_2 = Q_{rad} - \frac{\partial \overline{\omega' h'}}{\partial p} \quad (3)$$

238 where $h = s + L_v q$ is the moist static energy. With the phase change of water vapor cancelled,
239 $Q_1 - Q_2$ represents the radiative effect and the vertical convergence of eddy fluxes.

240 Consistent with the diurnal cycles of precipitation, the observed clouds and large-scale
241 vertical velocity differ primarily in the morning between IOP1 and IOP2. In IOP1, the early
242 morning upward motion peaks at 700 hPa and extends to the upper troposphere around 200 hPa.
243 The early afternoon upward motion peaks at the upper troposphere and extends above 100 hPa.
244 Accordingly, clouds are mainly seen between 800 and 500 hPa in the early morning but
245 throughout the entire troposphere in the afternoon. In IOP2, morning convective systems are
246 generally limited to the lower levels, as shown by weak upward motion below 600 hPa and
247 downward motion above. Thus, few clouds are observed in the lower and middle troposphere



248 while some high clouds remain from the previous day's convective activities. The afternoon
249 convective systems are strong and deep in both IOPs, with upward motion in the upper
250 troposphere associated with convective cloud growth and downward motion in the lower
251 troposphere associated with convective downdrafts.

252 Consistent with the clouds and vertical velocity, Figure 8 also shows significant seasonal
253 differences of Q_1 and Q_2 profiles in the morning, with heating and drying extending to the upper
254 troposphere in IOP1 but cooling and moistening above 600-650 hPa in IOP2. In the afternoon,
255 both IOPs show strong heating and drying in the middle and upper troposphere with weak
256 heating and strong moistening occurring below 700 hPa. The low-level heating and moistening
257 feature has been observed in trade wind regimes during westerly wind bursts and monsoon break
258 periods (Nitta and Esbensen, 1974; Lin and Johnson, 1996; Johnson and Lin, 1997; Xie et al.,
259 2010a), in which the vertical convergence of eddy fluxes and detrainment of shallow cumulus
260 were considered as the causes. In this study it is also seen in the afternoon precipitating periods
261 (red lines in Figure 5 and 6). The last row in Figure 8 shows $Q_1 - Q_2$ where two positive centers
262 are seen during daytime at ~750 to 950 hPa and ~250 to 550 hPa, respectively. Considering the
263 two terms in the right-hand-side of Eq. (3), the troposphere usually has a radiative cooling effect
264 and therefore Q_{rad} is usually negative. The positive $Q_1 - Q_2$ has to be due to the vertical
265 convergence of eddy fluxes of moist static energy associated with convective process, where
266 positive Q_1 comes from vertical convergence of dry static energy flux, and negative Q_2 comes
267 from vertical convergence of moisture flux.

268

269 6. Case Studies



270 A set of case studies is conducted to further understand the large-scale vertical velocity
271 and heat and moisture budgets for the three typical types of convective systems that often occur
272 in the wet season in Amazonia: locally-occurring systems (LOS), coastal-occurring systems
273 (COS), and basin-occurring systems (BOS). Previous studies have found that LOS often occur
274 in the afternoon characterized as scattered convections generated through solar heating at the
275 surface, while most COS and BOS are propagating systems associated with mid-level easterlies
276 and westerlies, respectively (e.g. Cifelli et al., 2002; Silva Dias et al., 2002a; Williams et al.,
277 2002), and affect Manaus in the early morning. COS occurring in easterlies are often westward
278 propagating squall-lines with intense leading lines that are more vertically developed. BOS
279 generated in the westerlies are generally less vertically developed MCSs with a broad horizontal
280 area and relatively homogeneous precipitation extending over a long time (Cifelli et al., 2002).
281 Table 1 gives the number of each type of precipitation system observed during the two IOPs,
282 identified from the radar loop (available at
283 https://www.youtube.com/playlist?list=PLVqbwaasmlvtcu2kl_U5RaaNF0kYqW6ua) and the satellite
284 infrared images (available at <http://www-pm.larc.nasa.gov/>). The two BOS cases identified in
285 IOP2 both occurred in the Amazon basin, but their structures are more like COS as squall lines
286 propagating westward. There are more COS and BOS in IOP1 than in IOP2, but the number of
287 afternoon LOS in IOP1 is just slightly higher than that in IOP2. This again indicates that the
288 frequency of morning propagating convective systems contributes to the variation of the diurnal
289 cycle between the wet and dry seasons.

290 The three selected cases are a LOS starting from 11 LT, 13 March 2014, a COS starting
291 from 2 LT, 20 March 2014 and a BOS starting from 17 LT, 1 March 2014. The times of these
292 events are marked by the black lines in Figure 3. Mid-level wind was dominated by westerlies



293 on 1 March (day 60) and easterlies on 20 March (day 79). Figure 9 shows representative scans
294 of the radar reflectivity at elevation angle of 0.9° for these three cases, as well as the time series
295 of the domain mean precipitation. The LOS case has many small-scale scattered convective cells
296 that last for very short times (typically a couple of hours). Because of the small horizontal
297 coverage of the convective cells, the domain mean precipitation is less than that in the other two
298 cases. The COS case has a clear bow-shape echo indicating a squall line front. The horizontal
299 size of the precipitating system is about 100 km and it moves quickly westward. The BOS case
300 has a much larger horizontal area of moderate precipitation with some embedded convective
301 cells. It moves southeastward and lasts more than 10 hours over the GoAmazon domain.

302 The point-observed cloud frequency and domain-averaged surface CAPE and CIN, u-
303 and v-winds, relative humidity, large-scale vertical velocity, Q_1 , and Q_2 for the three cases are
304 shown in Figures 10-12, respectively. For the LOS case, the cloud frequency is much smaller
305 than in the other two cases, since the convective cells have small horizontal extent and only
306 occupy a small portion of the region. A shallow-to-deep transition of convective clouds can be
307 seen. The surface CAPE is large, with weak mid-level winds and moist air at the surface before
308 the convection occurred. Upward motion corresponds to the deep convection, and the magnitude
309 is smaller than in the other two cases, consistent with weaker precipitation. Starting around 9 LT,
310 Q_1 shows diabatic heating throughout the troposphere during the deep convection, while Q_2
311 shows strong moistening between 750 and 950 hPa and weak drying above that layer. The
312 daytime moistening between 750 and 950 hPa due to the vertical convergence of eddy moisture
313 fluxes can also be seen on many other days during the two IOPs and was discussed in Section 5.
314 Note that there is a time lag between observed cloud frequency and the domain-averaged large-
315 scale fields, which might be partially due to the fact that the cloud frequency observations were



316 taken from vertically pointing instruments at the ARM site 67.8 km downwind of the center of
317 the GoAmazon domain.

318 The COS (Figure 11) and BOS (Figure 12) cases both show a shallow-to-deep convective
319 cloud transition from the previous evening to late afternoon, with a moist lower-level atmosphere.
320 Both cases have smaller surface CAPE than the LOS case, possibly because the convective
321 systems have released the atmospheric instability in the morning. The COS case passed through
322 the GoAmazon domain between 6 and 12 LT in strong mid-level easterlies, with deep clouds and
323 strong upward motion associated with the squall line. Stratiform clouds, associated with weak
324 upward motion, remained in the upper levels until ~16 LT. Condensation from the deep
325 convection contributes to strong diabatic heating and drying throughout the troposphere, while
326 after the passage of the squall line, a few isolated convective cells moved in and the large-scale
327 structure becomes similar to that in the LOS case, with upper-level heating and drying, low-level
328 heating and moistening. The BOS case entered the GoAmazon domain earlier than the COS case.
329 In weak mid-level westerlies and descending mid-to-low-level northerlies, the system moved
330 slowly southeastward and remained in the domain for a longer time. Strong upward motion
331 related to the MCS is seen from 18 to 6 LT. Large diabatic heating and drying related to the
332 strong condensation is also seen. The remnant high clouds were maintained until ~18 LT with
333 precipitation weakening over time. The upper-level heating and drying, lower-level cooling and
334 moistening indicate that there are precipitating stratiform clouds in the upper level and
335 evaporation of precipitation underneath.

336

337 7. Summary and Discussion



338 This study presented the characteristics of the seasonal variation and diurnal cycle of the
339 large-scale vertical velocity and diabatic heating (Q_1) and drying (Q_2) profiles for the two IOPs
340 conducted during the GoAmazon2014/5 experiment. A constrained variational analysis method
341 was used to derive the large-scale vertical velocity and Q_1 and Q_2 profiles based on surface and
342 TOA observations and ECMWF analysis. The derived profiles correspond well with observed
343 clouds and precipitation describing convective systems over Amazonia.

344 The large-scale environment over the region near Manaus has distinct seasonal variations
345 and diurnal cycles. The wet season (IOP1) has more frequent precipitation events than the dry
346 season (IOP2), especially in the morning. The large-scale upward motions during rainy periods
347 have similar strength in both IOPs, however, the peak level in IOP1 is much higher than that
348 exhibited in IOP2 (350 hPa vs. 550 hPa). Q_1 and Q_2 both have a double-peak feature during
349 rainy period, but the physical mechanism may be different: the double peak of Q_1 may be due to
350 the cooling near the melting level while the double peak of Q_2 may be due to the different height
351 of convective and stratiform systems. The seasonal contrast is mainly due to the higher
352 occurrence of morning mesoscale convective systems observed during IOP1. In the morning,
353 upward motion peaks at ~700 hPa and extends to the upper troposphere during IOP1, while it is
354 limited to the lower levels with downward motion at the upper levels during IOP2. Afternoon
355 convective systems have a higher vertical motion peak than their morning counterparts, and both
356 IOPs show similar vertical structures for the afternoon systems. The large-scale vertical velocity
357 shows upward motion above 700 hPa and downward motion below. Accordingly, Q_1 and Q_2
358 also exhibit middle and upper level heating and drying related to the deep convection. Below
359 750 hPa, the profiles show relatively weak heating and strong moistening. This heating and



360 moistening feature is due to the vertical convergence of eddy fluxes of heat and moisture in the
361 boundary layer.

362 Three cases from IOP1 representing different types of convective systems that often
363 occur in the region were chosen and analyzed in this study: locally-occurring systems (LOS),
364 coastal-occurring systems (COS) and basin-occurring systems (BOS). The LOS case was
365 characterized by many scattered and short-lived convective cells. It had relatively weak upward
366 motion, heating and drying in the free troposphere, and heating and moistening in the boundary
367 layer. The COS case occurred in strong mid-level easterlies. It was characterized as a squall line
368 with deep strong profiles of upward motion, heating and drying. The BOS case mainly happened
369 in weak mid-level westerlies and descending mid-to-low-level northerlies. It was characterized
370 as widespread, moderate precipitation with embedded convective cells, and lasted much longer
371 than the other two systems. The precipitating stratiform clouds remained at upper levels for
372 several hours evident by upper-level condensational heating and lower-level evaporative cooling.
373 The frequency of LOS cases is similar in both IOPs while the COS and BOS events occur much
374 more often during the wet season than the dry season. The seasonal variation of the diurnal cycle
375 of precipitation, clouds, and environmental variables is mainly due to the COS and BOS events
376 observed in the morning.

377 Previous studies have also shown that the river breeze has an important influence on the
378 diurnal cycle near the Amazon River (e.g. dos Santos et al., 2014; Tanaka et al., 2014; Burleyson
379 et al., 2016) and that the impact of the local circulation can extend as far as 50 km away from the
380 river. This local circulation and the horizontal inhomogeneity of large-scale vertical velocity,
381 heating, and moistening could be better studied using high-resolution 3-D gridded large-scale



382 forcing data from the three-dimensional constrained variational analysis recently developed by
383 Tang and Zhang (2015) and Tang et al. (2016). This will be the subject of a future study.

384

385 *Acknowledgment: The authors gratefully thank Luiz Machado, Jiwen Fan and many others in*
386 *the GoAmazon group for valuable discussions about the synoptic and climate features in*
387 *Amazonia region. This research is supported by the Biological and Environmental Research*
388 *Division in the Office of Sciences of the US Department of Energy (DOE). Work at LLNL was*
389 *supported by the DOE Atmospheric Radiation Measurement (ARM) program and performed*
390 *under the auspices of the U. S. Department of Energy by Lawrence Livermore National*
391 *Laboratory under contract No. DE-AC52-07NA27344. Work at Stony Brook was supported by*
392 *the Office of Science of the U. S. Department of Energy and by the National Science Foundation.*
393 *This manuscript has been authored by employees of Brookhaven Science Associates, LLC with*
394 *support from the ARM program and Atmospheric Systems Research Program under Contract No.*
395 *DE-AC02-98CH10886 with the U.S. Department of Energy. Dr. Zhe Feng at the Pacific*
396 *Northwest National Laboratory (PNNL) is supported by the U.S. DOE, as part of the*
397 *Atmospheric System Research (ASR) Program. PNNL is operated for DOE by Battelle Memorial*
398 *Institute under contract DE-AC05-76RL01830. The satellite analyses are supported by the DOE*
399 *ARM and ASR Program under contract, DE-SC0013896. The publisher by accepting the*
400 *manuscript for publication acknowledges that the United States Government retains a non-*
401 *exclusive, paid-up, irrevocable, world-wide license to publish or reproduce the published form of*
402 *this manuscript, or allow others to do so, for United States Government purposes. We thank The*
403 *Brazilian National Institute of Amazonian Research (INPA), the Amazonas State University*
404 *(UEA) and Dr. Antonio Manzi for providing surface flux data.*

405 **References**

- 406 Atmospheric Radiation Measurement (ARM) Climate Research Facility, updated hourly.
407 Radiative Flux Analysis (RADFLUX1LONG). 2014-02-15 to 2014-10-10, 3.21297 S 60.5981
408 W: ARM Mobile Facility (MAO) Manacapuru, Amazonas, Brazil; AMF1 (M1). Compiled by C.
409 Long, K. Gaustad and L. Riihimaki. Atmospheric Radiation Measurement (ARM) Climate
410 Research Facility Data Archive: Oak Ridge, Tennessee, USA. Data set accessed 2016-03-09 at
411 doi: 10.5439/1179822, 1994.
- 412 Atmospheric Radiation Measurement (ARM) Climate Research Facility, updated hourly. Quality
413 Controlled Eddy Correlation Flux Measurement (30QCECOR). 2014-02-15 to 2014-10-10,
414 3.21297 S 60.5981 W: ARM Mobile Facility (MAO) Manacapuru, Amazonas, Brazil; AMF1
415 (M1). Compiled by R. McCoy, Y. Zhang and S. Xie. Atmospheric Radiation Measurement
416 (ARM) Climate Research Facility Data Archive: Oak Ridge, Tennessee, USA. Data set accessed
417 2016-03-22 at doi: 10.5439/1097546, 2003.
- 418 Burleyson, C. D., Feng, Z., Hagos, S., Fast, J., Machado, L. A. T., and Martin, S. T.: Spatial
419 variability of the background diurnal cycle of deep convection around the GoAmazon2014/5
420 field campaign sites, *Journal of Applied Meteorology and Climatology*, in revision, doi, 2016.
- 421 Cifelli, R., Petersen, W. A., Carey, L. D., Rutledge, S. A., and da Silva Dias, M. A. F.: Radar
422 observations of the kinematic, microphysical, and precipitation characteristics of two MCSs in
423 TRMM LBA, *Journal of Geophysical Research: Atmospheres*, 107, LBA 44-41-LBA 44-16, doi:
424 10.1029/2000JD000264, 2002.
- 425 Cressman, G. P.: AN OPERATIONAL OBJECTIVE ANALYSIS SYSTEM, *Monthly Weather*
426 *Review*, 87, 367-374, doi: doi:10.1175/1520-0493(1959)087<0367:AOOAS>2.0.CO;2, 1959.
- 427 Cutrim, E. M. C., Martin, D. W., Butzow, D. G., Silva, I. M., and Yulaeva, E.: Pilot Analysis of
428 Hourly Rainfall in Central and Eastern Amazonia, *Journal of Climate*, 13, 1326-1334, doi:
429 10.1175/1520-0442(2000)013<1326:PAOHRI>2.0.CO;2, 2000.
- 430 Dee, D. P., Uppala, S. M., Simmons, A. J., Berrisford, P., Poli, P., Kobayashi, S., Andrae, U.,
431 Balmaseda, M. A., Balsamo, G., Bauer, P., Bechtold, P., Beljaars, A. C. M., van de Berg, L.,
432 Bidlot, J., Bormann, N., Delsol, C., Dragani, R., Fuentes, M., Geer, A. J., Haimberger, L., Healy,
433 S. B., Hersbach, H., Hólm, E. V., Isaksen, L., Kållberg, P., Köhler, M., Matricardi, M., McNally,
434 A. P., Monge-Sanz, B. M., Morcrette, J. J., Park, B. K., Peubey, C., de Rosnay, P., Tavolato, C.,
435 Thépaut, J. N., and Vitart, F.: The ERA-Interim reanalysis: configuration and performance of the
436 data assimilation system, *Quarterly Journal of the Royal Meteorological Society*, 137, 553-597,
437 doi: 10.1002/qj.828, 2011.



- 438 dos Santos, M. J., Silva Dias, M. A. F., and Freitas, E. D.: Influence of local circulations on wind,
439 moisture, and precipitation close to Manaus City, Amazon Region, Brazil, *Journal of*
440 *Geophysical Research: Atmospheres*, 119, 13,233-213,249, doi: 10.1002/2014JD021969, 2014.
- 441 Fu, R., Dickinson, R. E., Chen, M., and Wang, H.: How Do Tropical Sea Surface Temperatures
442 Influence the Seasonal Distribution of Precipitation in the Equatorial Amazon?, *Journal of*
443 *Climate*, 14, 4003-4026, doi: doi:10.1175/1520-0442(2001)014<4003:HDTSSST>2.0.CO;2, 2001.
- 444 Greco, S., Swap, R., Garstang, M., Ulanski, S., Shipham, M., Harriss, R. C., Talbot, R., Andreae,
445 M. O., and Artaxo, P.: Rainfall and surface kinematic conditions over central Amazonia during
446 ABLE 2B, *Journal of Geophysical Research: Atmospheres*, 95, 17001-17014, doi:
447 10.1029/JD095iD10p17001, 1990.
- 448 Hack, J. J., and Schubert, W. H.: Some dynamical properties of idealized thermally-forced
449 meridional circulations in the tropics, *Meteorol. Atmos. Phys.*, 44, 101-117, doi:
450 10.1007/BF01026813, 1990.
- 451 Harriss, R. C., Wofsy, S. C., Garstang, M., Browell, E. V., Molion, L. C. B., McNeal, R. J.,
452 Hoell, J. M., Bendura, R. J., Beck, S. M., Navarro, R. L., Riley, J. T., and Snell, R. L.: The
453 Amazon Boundary Layer Experiment (ABLE 2A): dry season 1985, *Journal of Geophysical*
454 *Research: Atmospheres*, 93, 1351-1360, doi: 10.1029/JD093iD02p01351, 1988.
- 455 Harriss, R. C., Garstang, M., Wofsy, S. C., Beck, S. M., Bendura, R. J., Coelho, J. R. B., Drewry,
456 J. W., Hoell, J. M., Matson, P. A., McNeal, R. J., Molion, L. C. B., Navarro, R. L., Rabine, V.,
457 and Snell, R. L.: The Amazon Boundary Layer Experiment: Wet season 1987, *Journal of*
458 *Geophysical Research: Atmospheres*, 95, 16721-16736, doi: 10.1029/JD095iD10p16721, 1990.
- 459 Hartmann, D. L., Hendon, H. H., and Houze, R. A.: Some Implications of the Mesoscale
460 Circulations in Tropical Cloud Clusters for Large-Scale Dynamics and Climate, *Journal of the*
461 *Atmospheric Sciences*, 41, 113-121, doi: 10.1175/1520-
462 0469(1984)041<0113:SIOTMC>2.0.CO;2, 1984.
- 463 Janowiak, J. E., Kousky, V. E., and Joyce, R. J.: Diurnal cycle of precipitation determined from
464 the CMORPH high spatial and temporal resolution global precipitation analyses, *Journal of*
465 *Geophysical Research: Atmospheres*, 110, n/a-n/a, doi: 10.1029/2005JD006156, 2005.
- 466 Johnson, R. H., and Lin, X.: Episodic Trade Wind Regimes over the Western Pacific Warm Pool,
467 *Journal of the Atmospheric Sciences*, 54, 2020-2034, doi: 10.1175/1520-
468 0469(1997)054<2020:ETWROT>2.0.CO;2, 1997.
- 469 Khaiyer, M., Minnis, P., Doelling, D. R., Nordeen, M. L., Palikonda, R., Rutan, D. A., and Yi, Y.:
470 Improved TOA broadband shortwave and longwave fluxes derived from satellites over the
471 Tropical Western Pacific, 13th Conference on Atmospheric Radiation, Am. Meteorol. Soc.,
472 Portland, OR. 27 June to 2 July, 2010.



- 473 Kollias, P., Miller, M. A., Luke, E. P., Johnson, K. L., Clothiaux, E. E., Moran, K. P., Widener,
474 K. B., and Albrecht, B. A.: The Atmospheric Radiation Measurement Program Cloud Profiling
475 Radars: Second-Generation Sampling Strategies, Processing, and Cloud Data Products, *Journal*
476 *of Atmospheric and Oceanic Technology*, 24, 1199-1214, doi: 10.1175/JTECH2033.1, 2007.
- 477 Lau, K. M., and Peng, L.: Origin of Low-Frequency (Intraseasonal) Oscillations in the Tropical
478 Atmosphere. Part I: Basic Theory, *Journal of the Atmospheric Sciences*, 44, 950-972, doi:
479 10.1175/1520-0469(1987)044<0950:OOLFOI>2.0.CO;2, 1987.
- 480 Li, W., Fu, R., and Dickinson, R. E.: Rainfall and its seasonality over the Amazon in the 21st
481 century as assessed by the coupled models for the IPCC AR4, *Journal of Geophysical Research:*
482 *Atmospheres*, 111, n/a-n/a, doi: 10.1029/2005JD006355, 2006.
- 483 Lin, X., and Johnson, R. H.: Heating, Moistening, and Rainfall over the Western Pacific Warm
484 Pool during TOGA COARE, *Journal of the Atmospheric Sciences*, 53, 3367-3383, doi:
485 10.1175/1520-0469(1996)053<3367:HMAROT>2.0.CO;2, 1996.
- 486 Machado, L. A. T., Laurent, H., Dessay, N., and Miranda, I.: Seasonal and diurnal variability of
487 convection over the Amazonia: A comparison of different vegetation types and large scale
488 forcing, *Theor Appl Climatol*, 78, 61-77, doi: 10.1007/s00704-004-0044-9, 2004.
- 489 Machado, L. A. T., Silva Dias, M. A. F., Morales, C., Fisch, G., Vila, D., Albrecht, R., Goodman,
490 S. J., Calheiros, A. J. P., Biscaro, T., Kummerow, C., Cohen, J., Fitzjarrald, D., Nascimento, E.
491 L., Sakamoto, M. S., Cunningham, C., Chaboureau, J.-P., Petersen, W. A., Adams, D. K.,
492 Baldini, L., Angelis, C. F., Sapucci, L. F., Salio, P., Barbosa, H. M. J., Landulfo, E., Souza, R. A.
493 F., Blakeslee, R. J., Bailey, J., Freitas, S., Lima, W. F. A., and Tokay, A.: The Chuva Project:
494 How Does Convection Vary across Brazil?, *Bulletin of the American Meteorological Society*, 95,
495 1365-1380, doi: 10.1175/BAMS-D-13-00084.1, 2014.
- 496 Marengo, J. A., Liebmann, B., Grimm, A. M., Misra, V., Silva Dias, P. L., Cavalcanti, I. F. A.,
497 Carvalho, L. M. V., Berbery, E. H., Ambrizzi, T., Vera, C. S., Saulo, A. C., Nogues-Paegle, J.,
498 Zipser, E., Seth, A., and Alves, L. M.: Recent developments on the South American monsoon
499 system, *International Journal of Climatology*, 32, 1-21, doi: 10.1002/joc.2254, 2012.
- 500 Martin, S. T., Artaxo, P., Machado, L. A. T., Manzi, A. O., Souza, R. A. F., Schumacher, C.,
501 Wang, J., Andreae, M. O., Barbosa, H. M. J., Fan, J., Fisch, G., Goldstein, A. H., Guenther, A.,
502 Jimenez, J. L., Pöschl, U., Silva Dias, M. A., Smith, J. N., and Wendisch, M.: Introduction:
503 Observations and Modeling of the Green Ocean Amazon (GoAmazon2014/5), *Atmos. Chem.*
504 *Phys.*, 16, 4785-4797, doi: 10.5194/acp-16-4785-2016, 2016.
- 505 Minnis, P., and Harrison, E. F.: Diurnal Variability of Regional Cloud and Clear-Sky Radiative
506 Parameters Derived from GOES Data. Part II: November 1978 Cloud Distributions, *Journal of*



- 507 Climate and Applied Meteorology, 23, 1012-1031, doi: doi:10.1175/1520-
508 0450(1984)023<1012:DVORCA>2.0.CO;2, 1984.
- 509 Minnis, P., and Smith, W. L.: Cloud and radiative fields derived from GOES-8 during SUCCESS
510 and the ARM-UAV spring 1996 flight series, Geophysical Research Letters, 25, 1113-1116, doi:
511 10.1029/98GL00301, 1998.
- 512 Nitta, T., and Esbensen, S.: Heat and Moisture Budget Analyses Using BOMEX Data, Monthly
513 Weather Review, 102, 17-28, doi: 10.1175/1520-0493(1974)102<0017:HAMBAU>2.0.CO;2,
514 1974.
- 515 Puri, K.: Some Experiments on the Use of Tropical Diabatic Heating Information for Initial State
516 Specification, Monthly Weather Review, 115, 1394-1406, doi: 10.1175/1520-
517 0493(1987)115<1394:SEOTUO>2.0.CO;2, 1987.
- 518 Schumacher, C., and Houze, R. A.: Stratiform Rain in the Tropics as Seen by the TRMM
519 Precipitation Radar*, Journal of Climate, 16, 1739-1756, doi: 10.1175/1520-
520 0442(2003)016<1739:SRITTA>2.0.CO;2, 2003.
- 521 Schumacher, C., Zhang, M. H., and Ciesielski, P. E.: Heating Structures of the TRMM Field
522 Campaigns, Journal of the Atmospheric Sciences, 64, 2593-2610, doi: 10.1175/JAS3938.1, 2007.
- 523 Schumacher, C., Ciesielski, P. E., and Zhang, M. H.: Tropical Cloud Heating Profiles: Analysis
524 from KWAJEX, Monthly Weather Review, 136, 4289-4300, doi: 10.1175/2008MWR2275.1,
525 2008.
- 526 Silva Dias, M. A. F., Petersen, W., Silva Dias, P. L., Cifelli, R., Betts, A. K., Longo, M., Gomes,
527 A. M., Fisch, G. F., Lima, M. A., Antonio, M. A., and Albrecht, R. I.: A case study of convective
528 organization into precipitating lines in the Southwest Amazon during the WETAMC and
529 TRMM-LBA, Journal of Geophysical Research: Atmospheres, 107, LBA 46-41-LBA 46-23, doi:
530 10.1029/2001JD000375, 2002a.
- 531 Silva Dias, M. A. F., Rutledge, S., Kabat, P., Silva Dias, P. L., Nobre, C., Fisch, G., Dolman, A.
532 J., Zipser, E., Garstang, M., Manzi, A. O., Fuentes, J. D., Rocha, H. R., Marengo, J., Plana-
533 Fattori, A., Sá, L. D. A., Alvalá, R. C. S., Andreae, M. O., Artaxo, P., Gielow, R., and Gatti, L.:
534 Cloud and rain processes in a biosphere-atmosphere interaction context in the Amazon Region,
535 Journal of Geophysical Research: Atmospheres, 107, LBA 39-31-LBA 39-18, doi:
536 10.1029/2001JD000335, 2002b.
- 537 Tanaka, L. M. d. S., Satyamurty, P., and Machado, L. A. T.: Diurnal variation of precipitation in
538 central Amazon Basin, International Journal of Climatology, 34, 3574-3584, doi:
539 10.1002/joc.3929, 2014.



- 540 Tang, S., and Zhang, M.: Three-dimensional constrained variational analysis: Approach and
541 application to analysis of atmospheric diabatic heating and derivative fields during an ARM SGP
542 intensive observational period, *Journal of Geophysical Research: Atmospheres*, 120, 7283-7299,
543 doi: 10.1002/2015JD023621, 2015.
- 544 Tang, S., Zhang, M., and Xie, S.: An ensemble constrained variational analysis of atmospheric
545 forcing data and its application to evaluate clouds in CAM5, *Journal of Geophysical Research:*
546 *Atmospheres*, 121, 33-48, doi: 10.1002/2015JD024167, 2016.
- 547 Williams, E., Rosenfeld, D., Madden, N., Gerlach, J., Gears, N., Atkinson, L., Dunnemann, N.,
548 Frostrom, G., Antonio, M., Biazon, B., Camargo, R., Franca, H., Gomes, A., Lima, M., Machado,
549 R., Manhaes, S., Nachtigall, L., Piva, H., Quintiliano, W., Machado, L., Artaxo, P., Roberts, G.,
550 Renno, N., Blakeslee, R., Bailey, J., Boccippio, D., Betts, A., Wolff, D., Roy, B., Halverson, J.,
551 Rickenbach, T., Fuentes, J., and Avelino, E.: Contrasting convective regimes over the Amazon:
552 Implications for cloud electrification, *Journal of Geophysical Research: Atmospheres*, 107, LBA
553 50-51-LBA 50-19, doi: 10.1029/2001JD000380, 2002.
- 554 Xie, S., Cederwall, R. T., and Zhang, M.: Developing long-term single-column model/cloud
555 system-resolving model forcing data using numerical weather prediction products constrained by
556 surface and top of the atmosphere observations, *Journal of Geophysical Research*, 109, doi:
557 10.1029/2003jd004045, 2004.
- 558 Xie, S., Hume, T., Jakob, C., Klein, S. A., McCoy, R. B., and Zhang, M.: Observed Large-Scale
559 Structures and Diabatic Heating and Drying Profiles during TWP-ICE, *Journal of Climate*, 23,
560 57-79, doi: 10.1175/2009jcli3071.1, 2010a.
- 561 Xie, S., McCoy, R. B., Klein, S. A., Cederwall, R. T., Wiscombe, W. J., Jensen, M. P., Johnson,
562 K. L., Clothiaux, E. E., Gaustad, K. L., Long, C. N., Mather, J. H., McFarlane, S. A., Shi, Y.,
563 Golaz, J.-C., Lin, Y., Hall, S. D., McCord, R. A., Palanisamy, G., and Turner, D. D.: CLOUDS
564 AND MORE: ARM Climate Modeling Best Estimate Data, *Bulletin of the American*
565 *Meteorological Society*, 91, 13-20, doi: 10.1175/2009BAMS2891.1, 2010b.
- 566 Yanai, M., Esbensen, S., and Chu, J.-H.: Determination of Bulk Properties of Tropical Cloud
567 Clusters from Large-Scale Heat and Moisture Budgets, *Journal of the Atmospheric Sciences*, 30,
568 611-627, doi: 10.1175/1520-0469(1973)030<0611:DOBPOT>2.0.CO;2, 1973.
- 569 Zhang, M., and Lin, J.: Constrained Variational Analysis of Sounding Data Based on Column-
570 Integrated Budgets of Mass, Heat, Moisture, and Momentum: Approach and Application to
571 ARM Measurements, *Journal of the Atmospheric Sciences*, 54, 1503-1524, doi: 10.1175/1520-
572 0469(1997)054<1503:CVAOSD>2.0.CO;2, 1997.



573 Zhang, M., Lin, J., Cederwall, R. T., Yio, J. J., and Xie, S. C.: Objective Analysis of ARM IOP
574 Data: Method and Sensitivity, Monthly Weather Review, 129, 295-311, doi: 10.1175/1520-
575 0493(2001)129<0295:OAOAID>2.0.CO;2, 2001.

576



577

Figure and Table Captions:

578 Table 1: number of convective systems identified in the morning and afternoon during IOP1 and
579 IOP2.

580

581 Figure 1: The location of GoAmazon site (top) and the analysis domain for this study (bottom). The
582 SIPAM radar is located at Ponta Pelada (indicated by red pentagram). Locations of other cities and
583 measurement sites are also indicated.

584 Figure 2: The sea-level pressure (shaded) and 10-meter horizontal wind (vector) averaged for IOP1 (left)
585 and IOP2 (right). The pentagram indicates the location of GoAmazon site.

586 Figure 3: Domain averaged time series of (from top to bottom) horizontal (u) wind, meridional (v) wind,
587 relative humidity, cloud frequency (point observation at the ARM site) and precipitation for IOP1 (left)
588 and IOP2 (right). The blank areas in cloud frequency indicate missing data. The three straight black lines
589 in IOP1 show the three cases chosen in section 6.

590 Figure 4: The time series (top) and temporal mean profiles (bottom) of large-scale vertical velocity for
591 IOP1 (left) and IOP2 (right).

592 Figure 5: The time series (top) and temporal mean profiles (bottom) of apparent heating source Q_1 for
593 IOP1 (left) and IOP2 (right).

594 Figure 6: The time series (top) and temporal mean profiles (bottom) of apparent moisture sink Q_2 for
595 IOP1 (left) and IOP2 (right).

596 Figure 7: The diurnal cycle of precipitation (up) and CAPE and CIN (bottom) for both IOPs.

597 Figure 8: The diurnal cycle of (from top to bottom) cloud frequency, large-scale vertical velocity, Q_1 , Q_2
598 and $Q_1 - Q_2$ for IOP1 and IOP2. The black lines are zero-lines.

599 Figure 9: SIPAM radar reflectivity snapshots (left) and time series of domain-mean precipitation (right)
600 for three cases of precipitating systems. From top to bottom: LOS, COS and BOS. The black octagons
601 indicate the GoAmazon domain, and the red arrows indicate the propagating direction of the system.

602 Figure 10: The time series of (a) cloud frequency, (b) surface CAPE and CIN, (c) u wind, (d) v wind, (e)
603 relative humidity, (f) vertical velocity, (g) Q_1 and (h) Q_2 for the LOS case. The black lines are zero-lines.
604 The shaded and white areas in (b) indicate nighttime and daytime.

605 Figure 11: The time series of (a) cloud frequency, (b) surface CAPE and CIN, (c) u wind, (d) v wind, (e)
606 relative humidity, (f) vertical velocity, (g) Q_1 and (h) Q_2 for the COS case. The black lines are zero-lines.
607 The shaded and white areas in (b) indicate nighttime and daytime.

608 Figure 12: The time series of (a) cloud frequency, (b) surface CAPE and CIN, (c) u wind, (d) v wind, (e)
609 relative humidity, (f) vertical velocity, (g) Q_1 and (h) Q_2 for the BOS case. The black lines are zero-lines.
610 The shaded and white areas in (b) indicate nighttime and daytime.



	IOP1		IOP2	
	Morning	Afternoon	Morning	Afternoon
Locally Occurring Systems (LOS)	0	19	0	14
Coastal Occurring Systems (COS)	7	6	0	3
Basin Occurring Systems (BOS)	3	3*	2**	0

611 * the afternoon BOS are continued from the morning time.

612 ** the two BOS in IOP2 are initialized in the Amazon basin but propagating westward as squall
 613 lines.

614

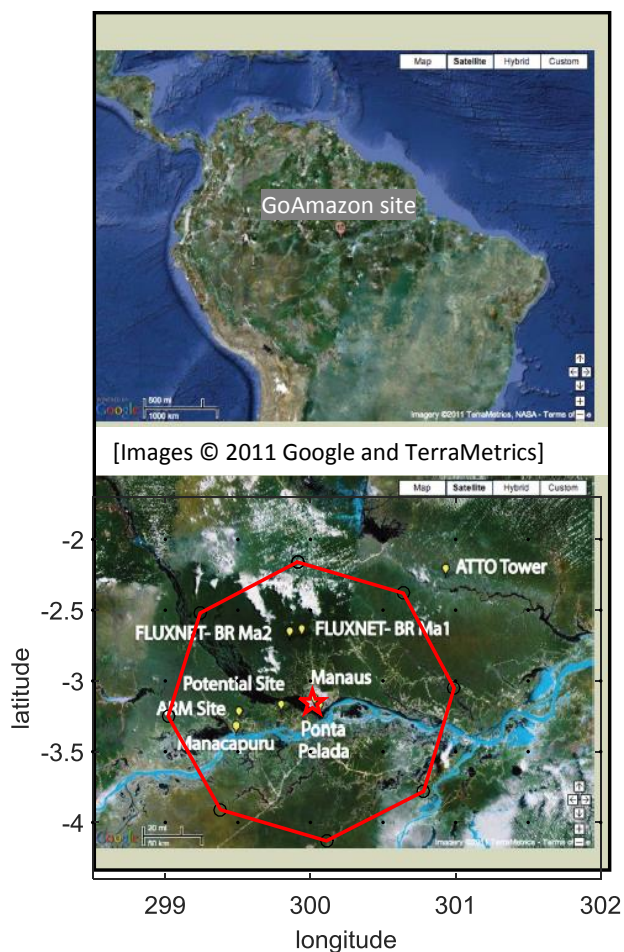
615 Table 1: number of convective systems identified in the morning and afternoon during IOP1 and
 616 IOP2.

617

618



619



620

621

622

623 Figure 1: The location of GoAmazon site (top) and the analysis domain for this study (bottom). The
624 SIPAM radar is located at Ponta Pelada (indicated by red pentagram). Locations of other cities and
625 measurement sites are also indicated.

626

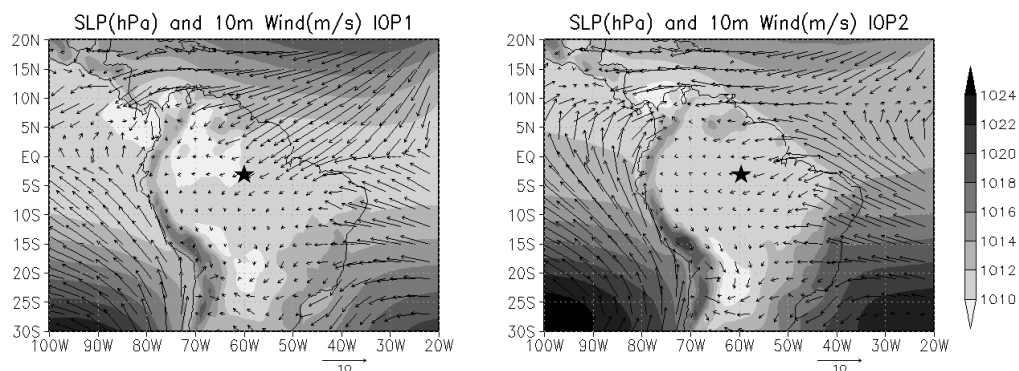
627

628



629

630



631

632 Figure 2: The sea-level pressure (shaded) and 10-meter horizontal wind (vector) averaged for IOP1 (left)
633 and IOP2 (right). The pentagram indicates the location of GoAmazon site.

634

635

636

637

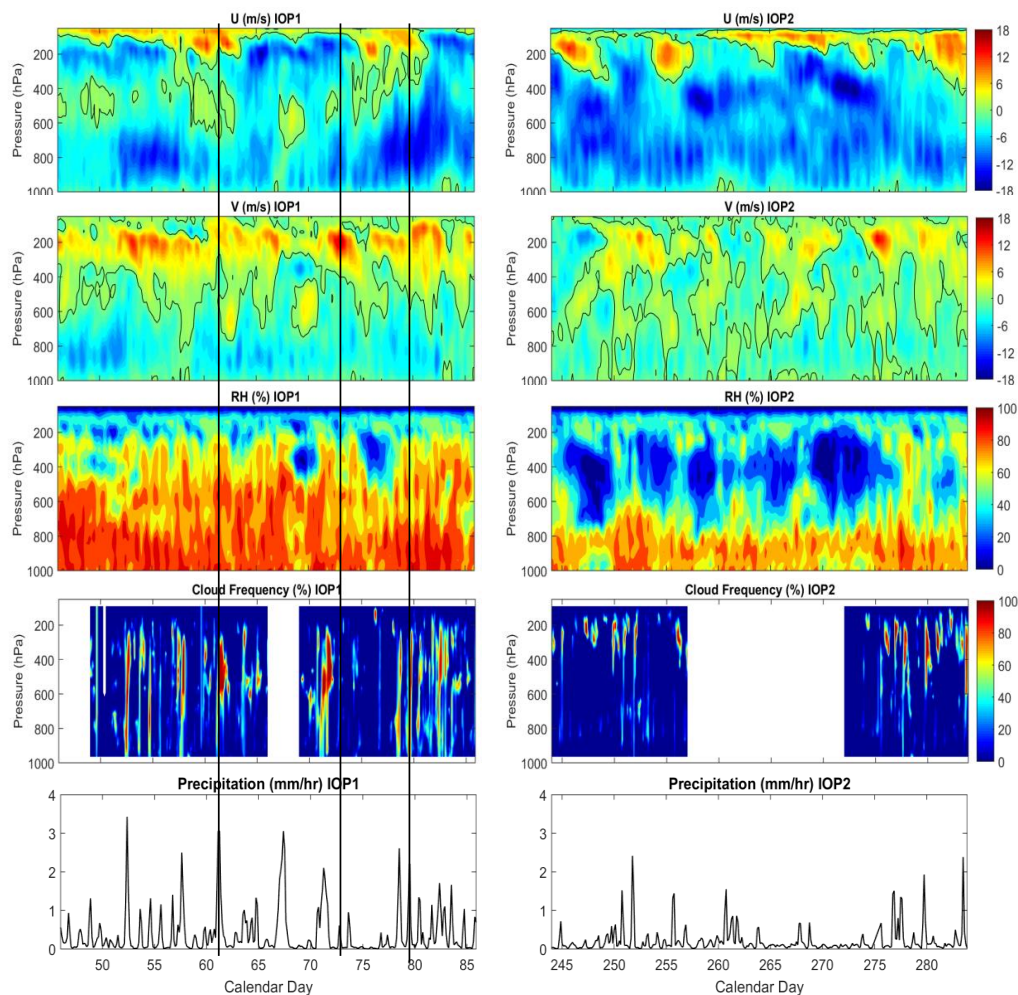
638



639

640

641



642

643 Figure 3: Domain averaged time series of (from top to bottom) horizontal (u) wind, meridional (v) wind,
644 relative humidity, cloud frequency (point observation at the ARM site) and precipitation for IOP1 (left)
645 and IOP2 (right). The blank areas in cloud frequency indicate missing data. The three straight black lines
646 in IOP1 show the three cases chosen in section 6.

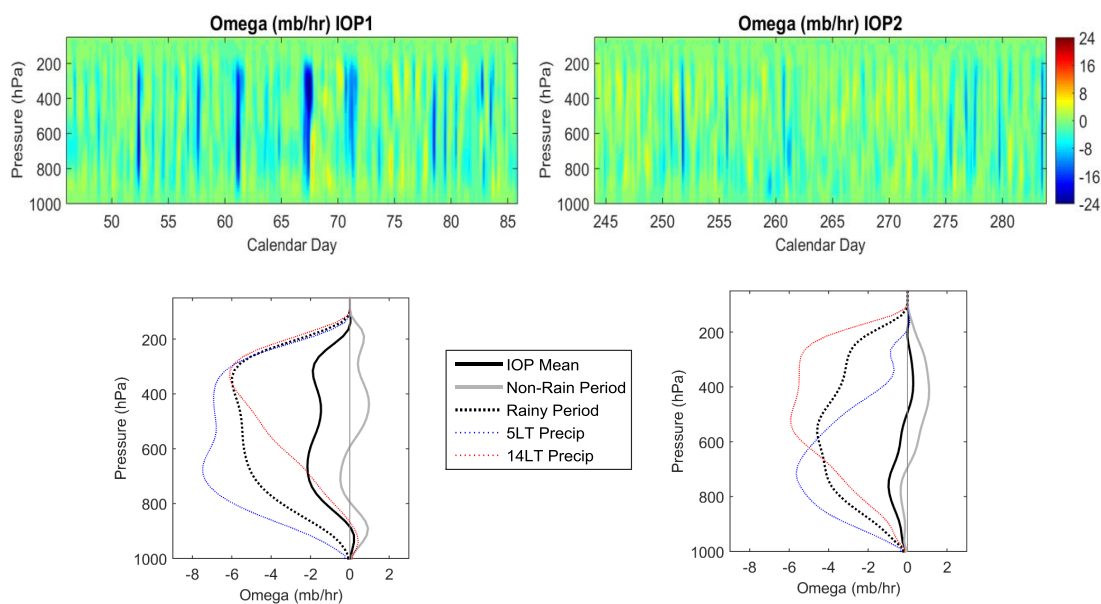
647



648

649

650



651

652

653

654 Figure 4: The time series (top) and temporal mean profiles (bottom) of large-scale vertical velocity for
655 IOP1 (left) and IOP2 (right).

656

657

658

659

660

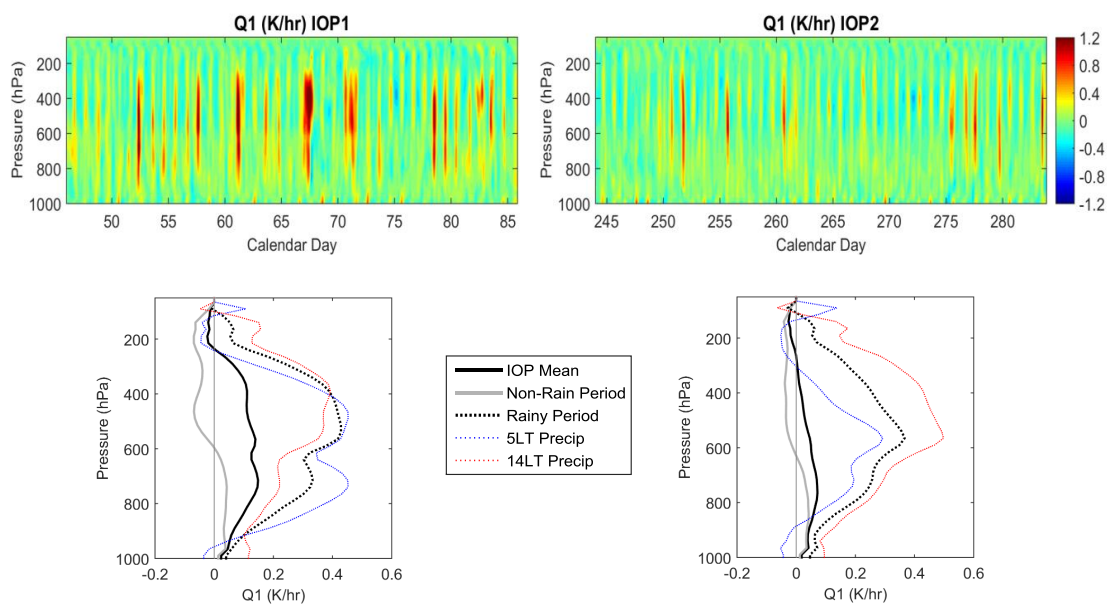
661

662

663



664



665

666

667

668 Figure 5: The time series (top) and temporal mean profiles (bottom) of apparent heating source Q_1 for
669 IOP1 (left) and IOP2 (right).

670

671

672

673

674

675

676

677

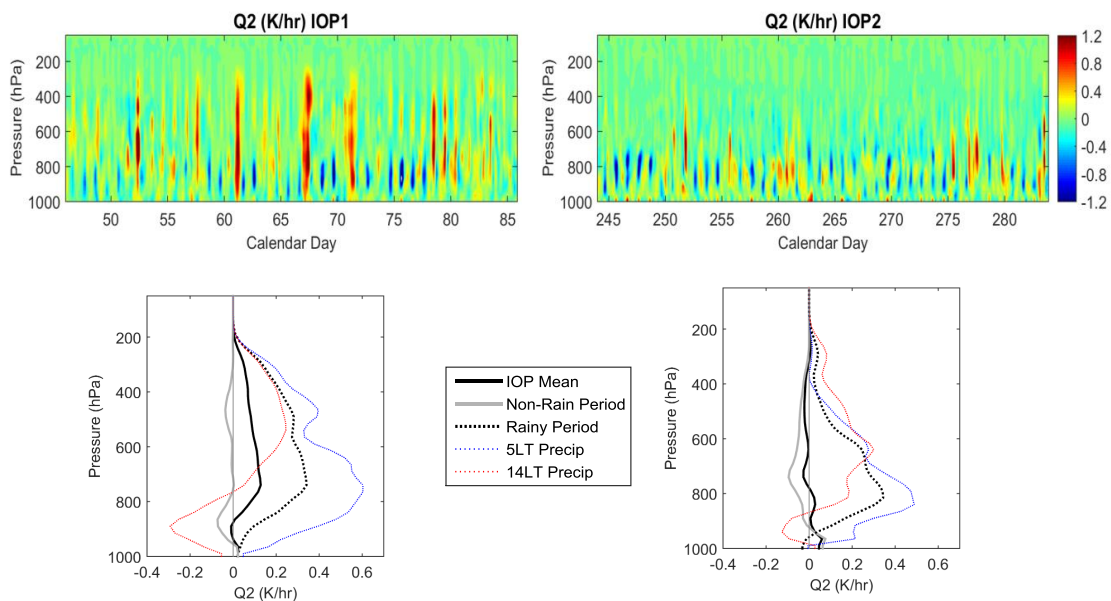
678

679



680

681



682

683 Figure 6: The time series (top) and temporal mean profiles (bottom) of apparent moisture sink Q_2 for
684 IOP1 (left) and IOP2 (right).

685

686

687

688

689

690

691

692

693

694

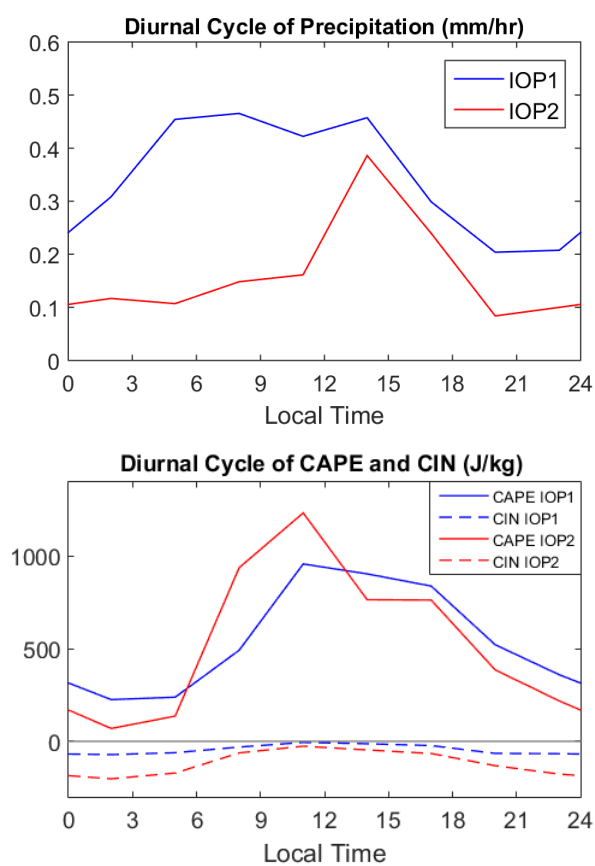
695



696

697

698



699

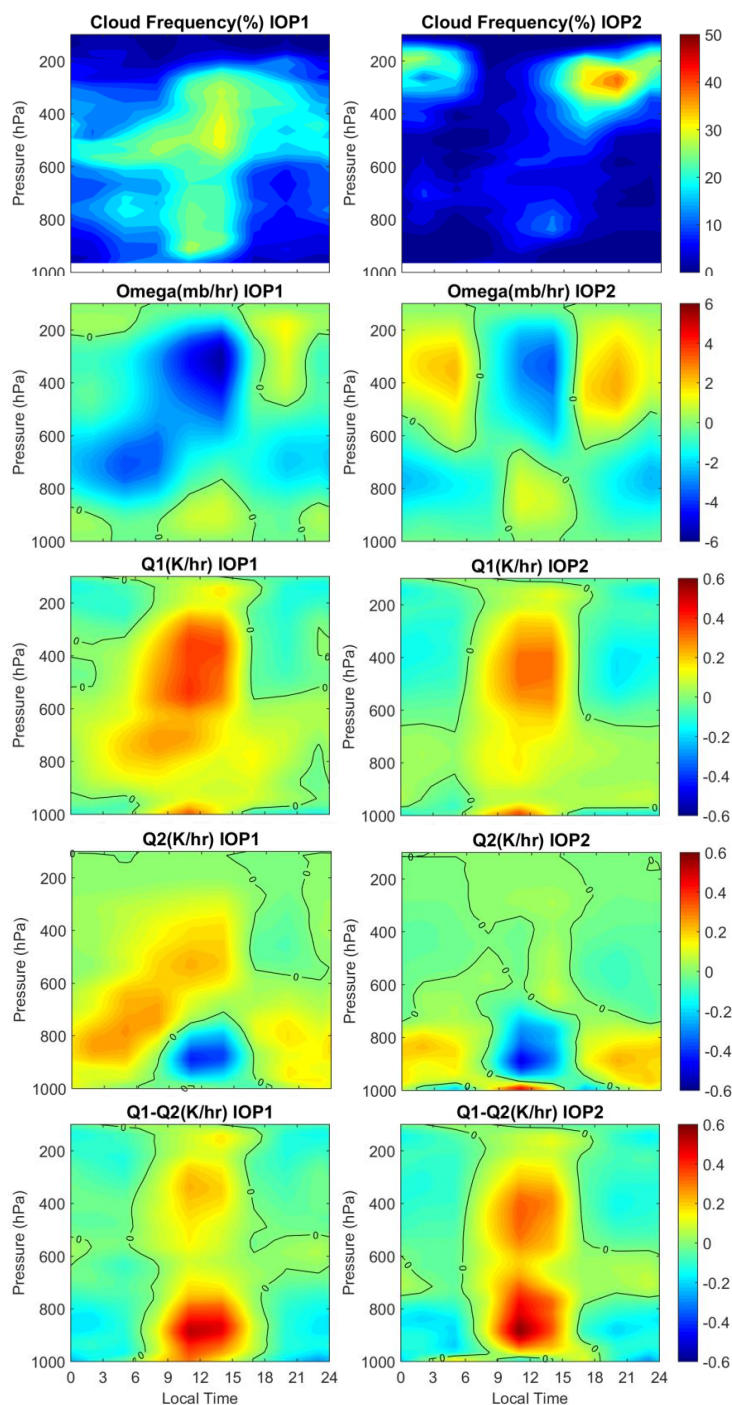
700 Figure 7: The diurnal cycle of precipitation (up) and CAPE and CIN (bottom) for both IOPs.

701

702

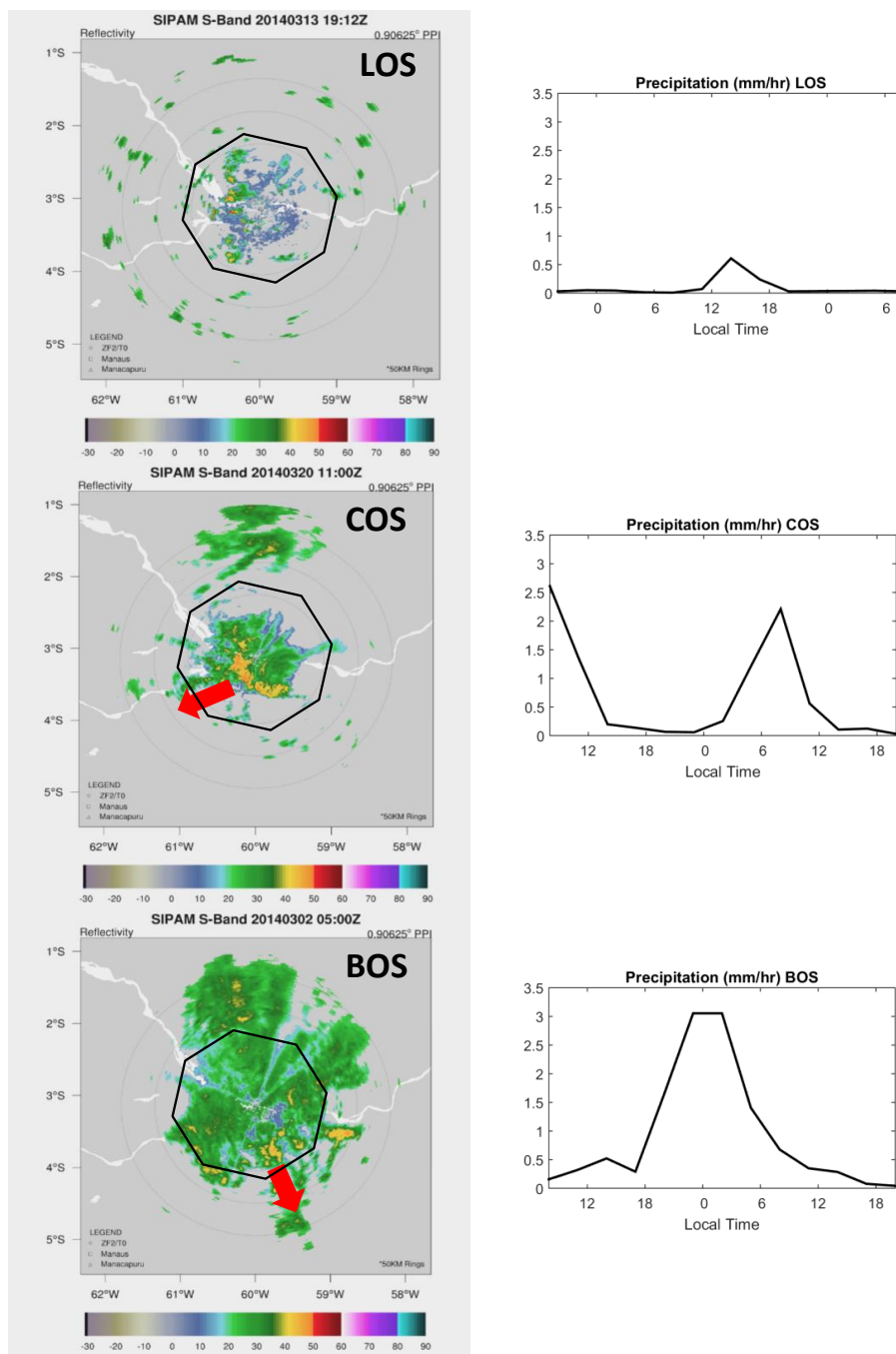
703

704



705

706 Figure 8: The diurnal cycle of (from top to bottom) cloud frequency, large-scale vertical velocity, Q_1 , Q_2
707 and $Q_1 - Q_2$ for IOP1 and IOP2. The black lines are zero-lines.



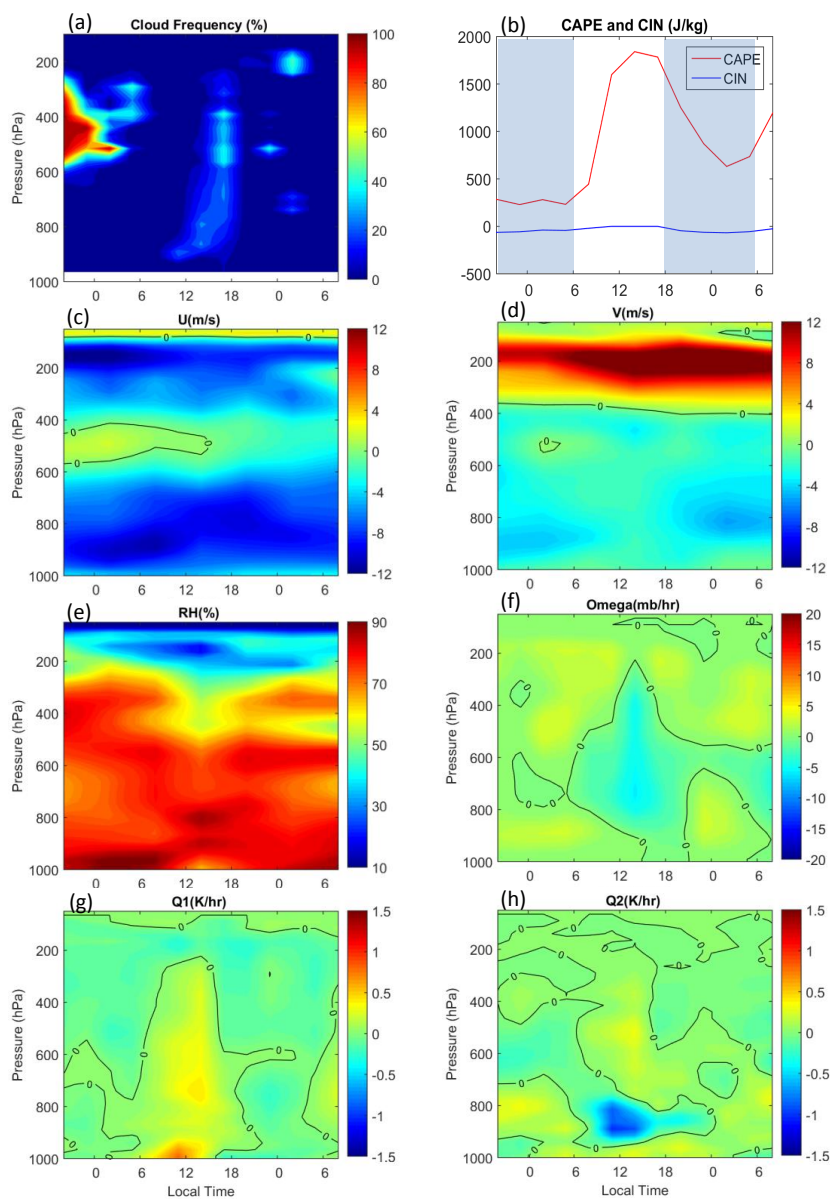
708

709 Figure 9: SIPAM radar reflectivity snapshots (left) and time series of domain-mean precipitation (right)
710 for three cases of precipitating systems. From top to bottom: LOS, COS and BOS. The black octagons
711 indicate the GoAmazon domain, and the red arrows indicate the propagating direction of the system.

712



LOS (14 March 2014)

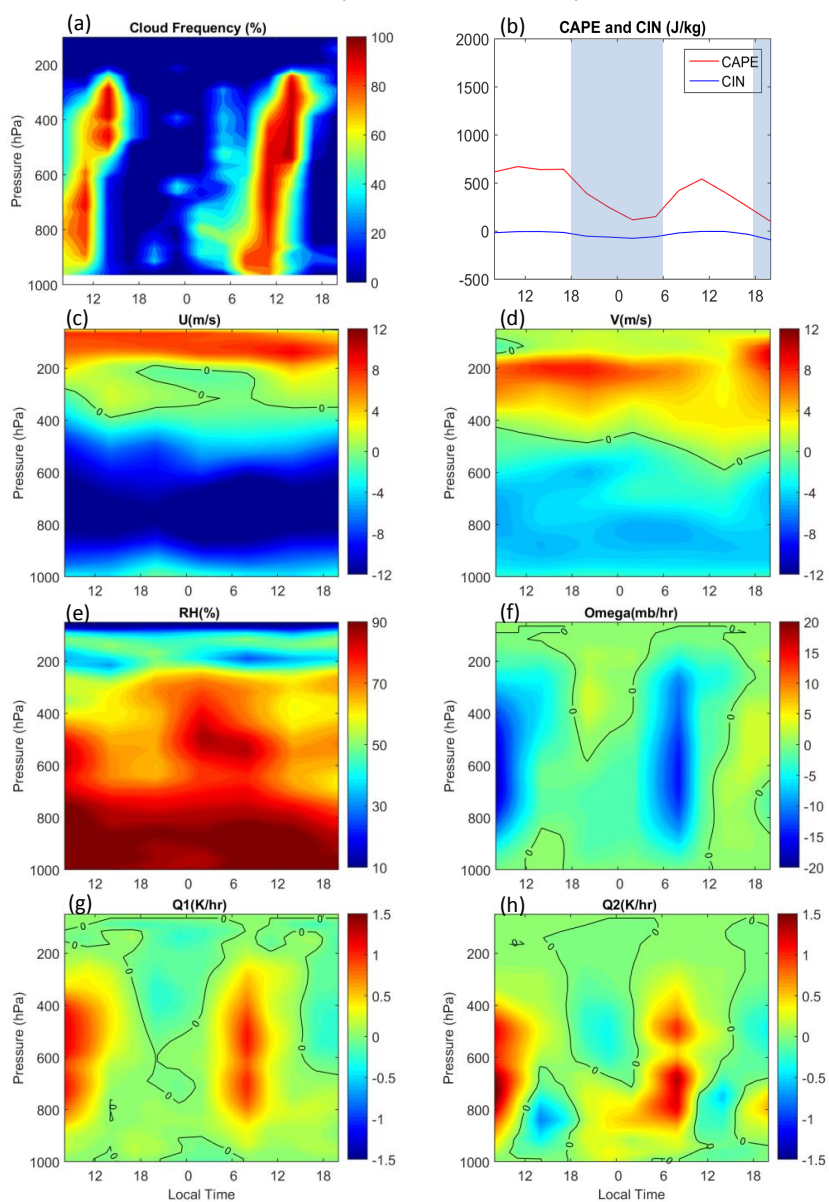


713

714 Figure 10: The time series of (a) cloud frequency, (b) surface CAPE and CIN, (c) u wind, (d) v wind, (e)
 715 relative humidity, (f) vertical velocity, (g) Q_1 and (h) Q_2 for the LOS case. The black lines are zero-lines.
 716 The shaded and white areas in (b) indicate nighttime and daytime.



COS (20 March 2014)



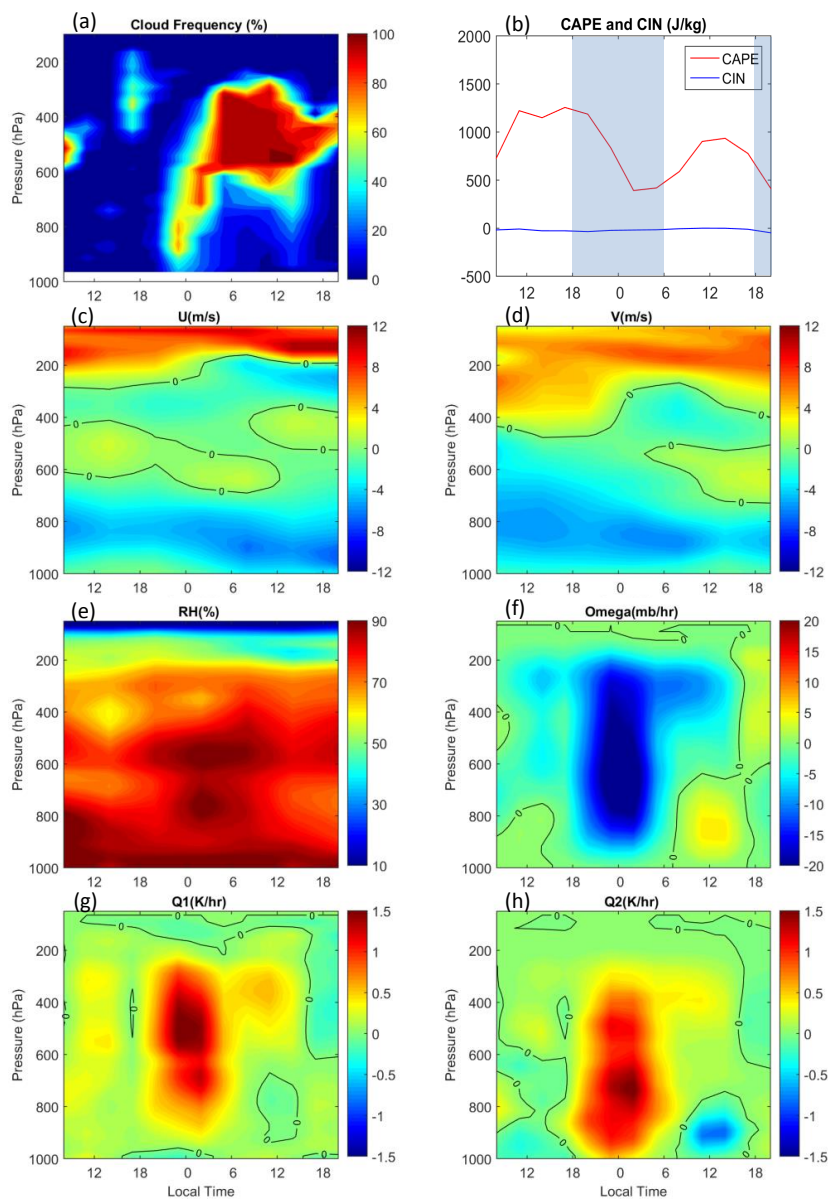
717

718 Figure 11: The time series of (a) cloud frequency, (b) surface CAPE and CIN, (c) u wind, (d) v wind, (e)
719 relative humidity, (f) vertical velocity, (g) Q_1 and (h) Q_2 for the COS case. The black lines are zero-lines.
720 The shaded and white areas in (b) indicate nighttime and daytime.

721



BOS (1 – 2 March 2014)



722

723 Figure 12: The time series of (a) cloud frequency, (b) surface CAPE and CIN, (c) u wind, (d) v wind, (e)
724 relative humidity, (f) vertical velocity, (g) Q_1 and (h) Q_2 for the BOS case. The black lines are zero-lines.
725 The shaded and white areas in (b) indicate nighttime and daytime.